Enhancement of oceanic uptake of anthropogenic CO_2 by macronutrient fertilization

Richard J. Matear and Bronwyn Elliott
CSIRO Marine Research, Hobart, Tasmania, Australia

Received 20 March 2000; revised 8 December 2003; accepted 30 December 2003; published 1 April 2004.

[1] A global three-dimensional ocean carbon cycle model was used to investigate the use of macronutrient fertilization of the ocean to increase the oceanic uptake of CO_2. To simulate macronutrient fertilization, phosphate was added to the 18°–50°S surface ocean. The carbon sequestration efficiency of fertilization was determined from the ratio of increased ocean uptake of anthropogenic CO_2 to the rate of phosphate addition to the upper ocean (converted to carbon units using the C/P ratio of organic matter, 106). The model simulation produced a maximum efficiency of 78%. However, the simulations demonstrated that changes in calcium carbon production with macronutrient fertilization could significantly reduce carbon sequestration efficiency. When calcium carbonate production increases at the same rate as export production, the carbon sequestration efficiency is reduced by 25% when compared to a simulation where calcium carbonate production is held constant. The study also discusses several other potential process that could impact the efficiency phosphate fertilization to sequester carbon in the ocean and the potential consequences of large-scale macronutrient fertilization of the ocean. *INDEX TERMS:* 4806 Oceanography: Biological and Chemical: Carbon cycling; 4842 Oceanography: Biological and Chemical: Modeling; 4845 Oceanography: Biological and Chemical: Nutrients and nutrient cycling; 4805 Oceanography: Biological and Chemical: Biogeochemical cycles (1615); *KEYWORDS:* CO_2, anthropogenic, uptake

Citation: Matear, R. J., and B. Elliott (2004), Enhancement of oceanic uptake of anthropogenic CO_2 by macronutrient fertilization, *J. Geophys. Res.*, *109*, C04001, doi:10.1029/2000JC000321.

1. Introduction

[2] The marine carbon cycle plays a major role in controlling atmospheric CO_2 levels. The oceans presently remove about 30% of the annual anthropogenic CO_2 emissions [*Battle et al.*, 2000; *Keeling et al.*, 1996]. Eventually the oceans will absorb about 80% of the total anthropogenic CO_2 emissions, but to attain this new equilibrium level of atmospheric CO_2 will take several thousand years. Given the importance of the ocean as a final reservoir of anthropogenic CO_2, it is natural to consider how one could accelerate the oceans' uptake of anthropogenic CO_2. Two proposed strategies exist for increasing the carbon sequestered by the ocean.

[3] One option is the direct deep-sea injection of CO_2. Modeling work of this option has shown that the ocean could absorb all the anthropogenic CO_2 present in the atmosphere and reduce the atmospheric CO_2 levels for many centuries [*Bacastow and Dewey*, 1996; *Wong and Matear*, 1997].

[4] A second option is to increase the uptake of carbon by the marine phytoplankton, thereby enhancing the biological "pumping" of carbon from the upper ocean into the deep sea [*Wong and Matear*, 1995]. This would then lower carbon levels in the upper ocean producing an additional flux of anthropogenic CO_2 from the atmosphere into the ocean. This enhancement of the biological pump could be accomplished through either iron fertilization or macronutrient fertilization. Iron fertilization is motivated by the observations that 25% of the surface ocean has ample macronutrients, which the marine phytoplankton do not completely utilize. Both shipboard incubations and large-scale iron additions have shown that biological production in these regions can be stimulated by adding iron [*Boyd et al.*, 1996; *Coale et al.*, 1996]. Modeling studies have assessed the potential of adding iron to the HNLC regions to sequester carbon [*Sarmiento and Orr*, 1991; *Kurz and Maier-Reimer*, 1993]. *Matear and Wong* [1999] calculated that iron fertilization of all HNLC regions for 100 years would enhance the oceanic uptake of CO_2 by 160Gt C. Box model studies by *Peng and Broecker* [1991] and *Joos et al.* [1991] give similar values for carbon sequester in the ocean by iron fertilization of the Southern Ocean.

[5] Marine production can also be increased by adding macronutrients to the upper ocean where macronutrient concentrations (phosphate and nitrate) are low and limit biological production. Approximately 70% of the surface ocean is macronutrient limited. The addition of macronutrients to these regions would stimulate biological activity and transfer organic carbon from the surface to the deep ocean.

[6] This study uses an Ocean Carbon Model (OCM) to assess the effect of macronutrient fertilization on oceanic CO_2 uptake. Our study is similar to an early modeling study

0148-0227/04/2000JC000321

of *Orr and Sarmiento* [1992]. The *Orr and Sarmiento* [1992] study showed that the atmospheric carbon sequestered by fertilizing the 18°–50°S region of the Southern Ocean was only 44% of the increase in export production. Such a result prompted these authors to conclude that macronutrient fertilization was an inefficient option for sequestering atmospheric CO_2. In the *Orr and Sarmiento* [1992] study, they simulated macronutrient fertilization by imposing a constant increase in export production in the fertilized region. In contrast, our study uses an ocean carbon model where export production is dependent on surface phosphate concentration and macronutrient fertilization is simulated by adding phosphate at a constant rate to the upper ocean. Our simulations of macronutrient fertilization enable one to simulate both the increase in export production and CO_2 uptake due to added phosphate. With our model we investigate the impact of macronutrient fertilization in the same 18°–50°S region of the Southern Ocean as the *Orr and Sarmiento* [1992] study.

[7] Two ocean carbon models are utilized in this study - 1) a box model of carbon and phosphate cycling and 2) a 3-D ocean carbon model (OCM). The box model provides a simple analytical model to elucidate the response of the ocean to macronutrient fertilization. The box model results provide the framework to interpret the results of the more realistic and more complex 3-D model. The 3-D ocean carbon model is used to investigate how the ocean would respond to macronutrient fertilization for both the present climate and the climate predicted by greenhouse warming. The simulations will be used to assess the efficiency of this option at sequestering anthropogenic CO_2 and the potential impacts of fertilization on ocean biogeochemical cycling and on marine ecosystems.

2. Box Model

[8] A two box model of the ocean was constructed to investigate macronutrient fertilization of a macronutrient-limited region In the box model, fertilization was simulated by adding phosphate to the surface box. Phosphate was added to the surface box at a constant rate, which stimulated the biological production in the surface box and the transfer of carbon from the surface box to the deep box. The carbon transport from the surface box to the deep box lowered carbon concentration of the surface box and resulted in a transfer of CO_2 from the atmosphere into the ocean. For this example, the atmospheric CO_2 concentration was fixed. The box model provides a means to estimate the efficiency of phosphate fertilization for a situation where phosphate limits biological export production.

[9] The evolution of phosphate (P) and DIC (C) in our two box model was modeled using the following equations where subscript 1 denotes values in the surface box and subscript 2 denotes values in the deep box:

$$\begin{aligned} V_1\frac{dP_1}{dt} &= a(P_2 - P_1) - bP_1 + eV_1 \\ V_2\frac{dP_2}{dt} &= -a(P_2 - P_1) + bP_1 \\ V_1\frac{dC_1}{dt} &= a(C_2 - C_1) - b\,r\,P_1 + f(C_{atm} - C_1) \\ V_2\frac{dC_2}{dt} &= -a(C_2 - C_1) - br\,P_1 \end{aligned} \quad . \tag{1}$$

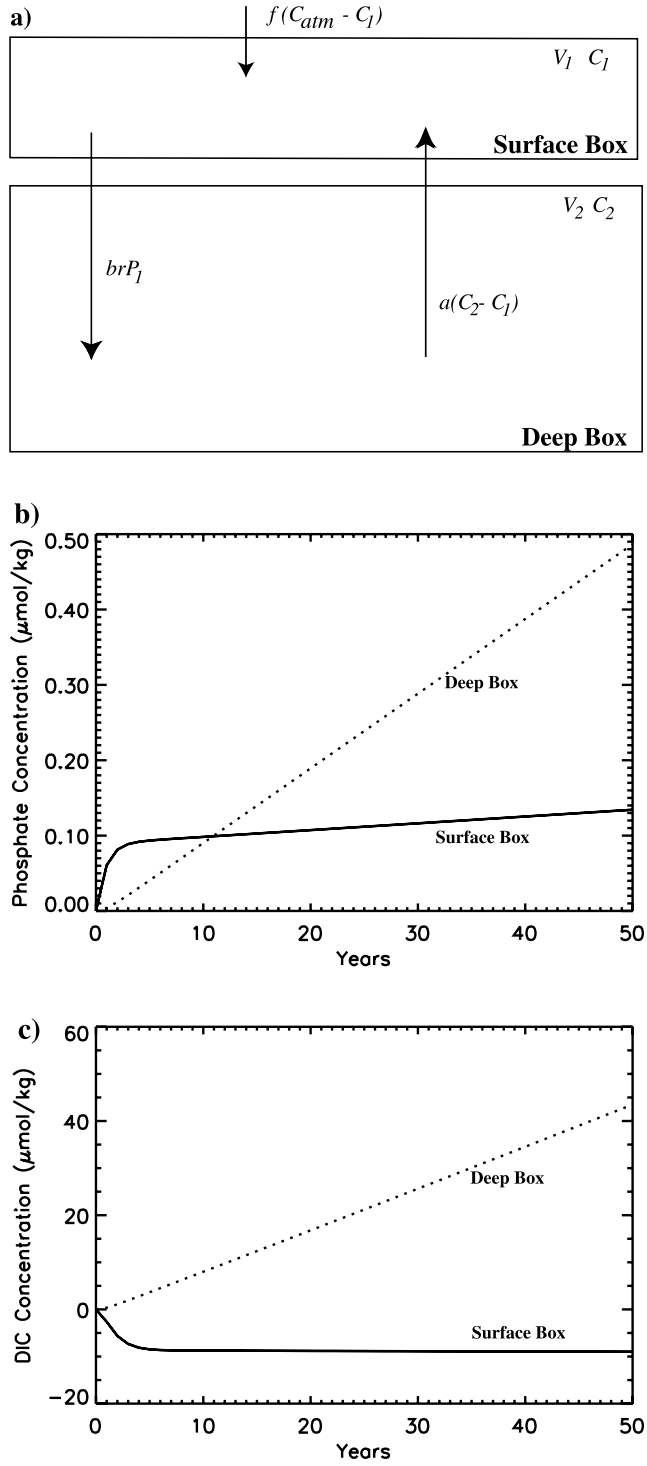

Figure 1. (a) Schematic of the box model for the evolution of dissolved inorganic carbon (DIC). For box model simulation with a phosphate fertilization rate of 0.1 μmol yr^{-1}, (b) change in the phosphate for the surface box (solid) and the deep box (dotted) and (c) change in DIC for the surface box (solid) and the deep box (dotted).

The evolution of P and C are affected by the vertical exchange between the two boxes (a), biological export production ($b\,P_1$), air-sea exchange of carbon dioxide ($f[C_{atm} - C_1]$) and the rate of phosphate fertilization (e) (Figure 1).

In the box model, export production is a linear function of phosphate concentration of the surface box(bP_1) and the air-sea exchange of CO_2 is determined by restoring the ocean surface box to a value in equilibrium with the atmosphere (C_{atm}). In (1), V is the volume of the boxes and r is the carbon to phosphate ratio of export production. The box model equations are linear, which enables one to treat separately the box model's response to fertilization from the model's response to increasing levels of atmospheric CO_2. For the simulations presented here we only look at fertilization affect by holding the atmospheric CO_2 level at constant value.

[10] Without fertilization ($e = 0$), the steady state solution to our box model is

$$\begin{aligned} P_1 &= \frac{aP_2}{a+b} \\ C_1 &= C_{atm} \\ C_2 &= C_{atm} + brP_1/a \end{aligned} \quad . \tag{2}$$

Parameter values appropriate for South Pacific subtropical gyre are $V_1 = 1$ and $V_2/V_1 = 10$, $r = 106$, $a = 0.1$ yr^{-1}, $b = 1$ yr^{-1} and $f = 1$ yr^{-1}, $P_2 = 2$ μmol kg^{-1}, $C_{atm} = 1900$ μmol kg^{-1}.

[11] Now, we simulate fertilization by adding phosphate to the surface box at a constant rate (e = 0.1 μmol kg^{-1} yr^{-1}). For the parameter values listed above, the evolution of phosphate and DIC in the two boxes rapidly adjust to a new state where P_1, P_2 and C_2 increase linearly with time and C_1 drops to a lower value (Figure 1).

[12] An analytical solution for the change in concentrations in the two boxes due to constant phosphate fertilization of the surface box can be found by assuming a solution for the concentrations are of the form $x\,t + y$. Where x and y are constants and t stands for time. The functional form of the solution is consistent with our simulation under a constant fertilization (Figure 1). Applying this assumption to our box model produced the following analytical solution:

$$\begin{aligned} \Delta P_1 &= \frac{eV_1(a\,t+V_2)}{a(V_1+V_2)+bV_2} \\ \Delta P_2 &= \frac{(a+b)eV_1}{a(V_1+V_2)+bV_2}t \\ \Delta C_1 &= -\frac{berV_1V_2}{(a(V_1+V_2)+bV_2)f} \\ \Delta C_2 &= \frac{berV_1(f\,t-V_2)}{(a(V_1+V_2)+bV_2)f} \end{aligned} \tag{3}$$

[13] The analytical solution shows that the carbon concentration in the surface box (C_1) does not change with time (consistent with numerical results shown in Figure 1 after the initial adjustment period). From the analytical solution, we can express the change in both export production and ocean uptake of carbon due to phosphate fertilization as follows

$$\begin{aligned} \Delta Export = rb\Delta P_1 &= \frac{reV_1(a\,t+V_2)}{a(V_1+V_2)+bV_2}b \\ \Delta Uptake = -f\Delta C_1 &= \frac{berV_1V_2}{(a(V_1+V_2)+bV_2)} \end{aligned} \quad . \tag{4}$$

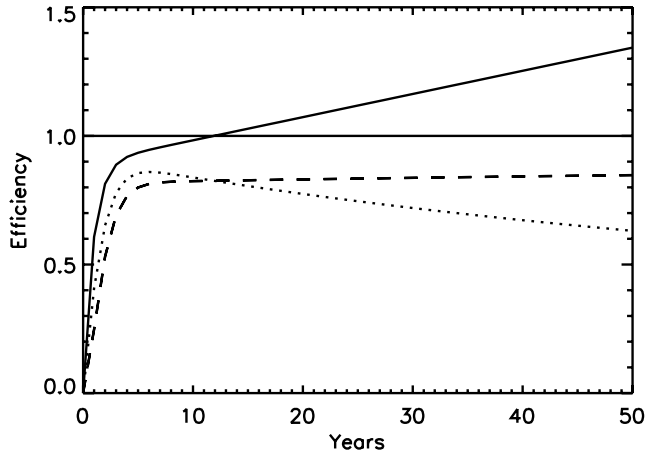

Figure 2. For the box model numerical simulation, the ratio of export production to phosphate addition multiplied by the C:P ratio, which is referred to as carbon equivalent units (solid), the ratio of CO_2 uptake to carbon export (dotted), and the ratio of CO_2 uptake to phosphate addition in carbon equivalent units (dashed).

[14] With constant phosphate fertilization, the export production grows linearly with time, but the oceanic uptake of carbon jumps to an elevated value that does not change with time. The growth in the export production with time, reflects the increased phosphate supply to the surface box from fertilization and from vertical supply of a phosphate-enriched deep box ($a[P_2 - P_1]$). The increased vertical supply of phosphate from the deep box increases export production, but does not alter the air-sea exchange of carbon, because the increased vertical supply of phosphate is associated with the increased vertical supply of carbon.

[15] With phosphate fertilization, the ratio of export production to the rate of phosphate fertilization is given as

$$\begin{aligned} \frac{\Delta Export}{Padded} &= \frac{eV_1(a\,t+V_2)}{a(V_1+V_2)+bV_2}rb/re \\ &= \frac{abV_1t}{(a(V_1+V_2)+bV_2)} + \frac{bV_1V_2}{(a(V_1+V_2)+bV_2)} \\ &\approx \frac{aV_1}{V_2}t\left(1-\frac{a}{b}\right) + V_1\left(1-\frac{a}{b}\right) \end{aligned} \quad . \tag{5}$$

The ratio is independent of the rate of phosphate addition (e) and it increases slowly with time as export production increases. For our model parameters, the growth rate is approximately 0.01 yr^{-1}. Figure 2 shows the evolution of this ratio from our numerical simulation ($e = 0.1$ μmol yr^{-1}).

[16] *Orr and Sarmiento* [1992] defined the efficiency of macronutrient fertilization at sequestering CO_2 as the ratio of increased carbon uptake to increased export production. For the box model, this definition of efficiency gives

$$\begin{aligned} Efficiency &= \frac{\Delta Uptake}{\Delta Export} \\ &= \frac{V_2}{a\,t+V_2} \end{aligned} \quad . \tag{6}$$

The efficiency decreases with time (Figure 2). Equation (6) is a poor measure of the carbon sequestration efficiency, because a fraction of the increase in export production is

due to increased vertical supply of phosphate to the surface box, which increases export production while having no effect on the ocean uptake of carbon. A better measure of the efficiency of phosphate fertilization is to compare the change in the ocean CO_2 uptake to the rate of phosphate addition in carbon equivalent units (i.e., phosphate addition multiplied by the C/P ratio, r, which equals re)

$$\frac{\Delta Uptake}{\Delta Padded} = \frac{berV_1V_2}{(a(V_1+V_2)+bV_2)}/re = \frac{bV_1V_2}{(a(V_1+V_2)+bV_2)} \approx V_1(1-a/b-aV_1/bV_2) \quad (7)$$

For our parameterization of export production (bP_1), the ratio is independent of the rate of phosphate addition. For the model parameters chosen for this South Pacific the ratio is approximately 0.89, which is slightly greater than the 0.86 value obtained from the numerical simulation (see Figure 2). As shown in Figure 2, once the box model has adjusted to the initial perturbation, the increased oceanic CO_2 uptake is approximately 86% of the phosphate addition (in equivalent carbon units).

3. Three-Dimensional Ocean Carbon Model

[17] The CSIRO Ocean Carbon Model (OCM) [*Matear and Hirst*, 1999] was used to make a more realistic assessment of the effectiveness of macronutrient fertilization at increasing oceanic CO_2 uptake. Our OCM determines the seasonal distribution of temperature, salinity, phosphate, oxygen, dissolved inorganic carbon and alkalinity by embedding a simple biogeochemical (BGC) module into an Ocean General Circulation Model (OGCM).

3.1. Ocean Circulation Model

[18] The ocean circulation model that we used was based on the Bryan-Cox OGCM [*Bryan*, 1984]. We use the model geometry of *Hirst and McDougall* [1996], which had a horizontal resolution of 3.186° longitude by 5.186° latitude and 21 vertical layers. The model bathymetry is a smoothed discretization of the real ocean bottom topography. In the model, horizontal and vertical viscosities are independent of depth and equal 50 and 2.5×10^9 cm^2 s^{-1} respectively. The profile of vertical mixing follows *Bryan and Lewis* [1979] with a value of 0.3 cm^2 s^{-1} at the surface, increasing to 1.3 cm^2 s^{-1} at 3500 m. Increased vertical diffusivity is used to mix regions of vertical instabilities. The Redi-Cox scheme [*Cox*, 1987] was used for isopycnal mixing with isopycnal diffusivity, K_i set to 10^7 cm^2 s^{-1}. The physical model uses the "GM" scheme [*Gent and McWilliams*, 1990; *Gent et al.*, 1995] for representing the adiabatic transport effects of baroclinic eddies. The diffusivity, which determines the strength of the eddy-induced transports, was set at 10^7 cm^2 s^{-1} [see *Rix and Willebrand*, 1996]. *England and Hirst* [1997] indicated that the temperature, salinity and CFC simulations were improved by the use of the GM scheme. *Matear* [2001] also showed that the natural ^{14}C simulation was improved with the GM scheme.

[19] The OGCM was forced with the monthly mean wind stress of *Hellerman and Rosenstein* [1983]. The surface flux of heat and salt were computed by restoring surface temperature and salinity to *Levitus* [1982] monthly mean values with a timescale of 30 d^{-1} and 50 d^{-1} for temperature and salinity respectively. The influence of the Mediterranean Sea was included in the model by having a diffusive flux of Mediterranean Sea water into the North Atlantic [*England et al.*, 1993]. In the high-latitude Southern Ocean, the salinity was restored to the observed winter values rather than the annual mean values [*England et al.*, 1993].

3.2. Ocean Biogeochemical Model

[20] The BGC module computed sources and sinks of the BGC tracers, which were then incorporated, into the tracer equations of the respective tracers. The tracer equation for the BGC tracers was identical to the temperature and salinity equations except for the inclusion of the BGC sources and sink terms, Q. In an idealized form, the tracer equation for BGC tracers was

$$\frac{\partial C}{\partial t} + \nabla\cdot(uC) = \nabla\cdot(K_h\nabla C) + \frac{\partial}{\partial z}\cdot\left(K_z\frac{\partial C}{\partial z}\right) + Q \quad (8)$$

where C represents the tracer concentration, $\boldsymbol{u}$ is the 3-D velocity, K_h and K_v are the horizontal and vertical diffusion coefficients (which include isopycnal and GM mixing terms) and Q represents the source/sinks due to biological processes and air-sea exchanges.

[21] In the model, biological production (photosynthesis) only occurred in the euphotic zone, which is set to the surface layer of the ocean model (upper 50 m). The export of organic matter (EP) from the euphotic zone was determined using the following equation.

$$EP = S\left(\frac{I}{I_o}\right)\left(\frac{h_e}{h}\right)\left(\frac{P}{P+P_o}\right)(1.066)^T, P_o = 0.1\ \mu\text{mol/kg}. \quad (9)$$

where S is the scaling factor in mol C m^{-2} s^{-1}, I is the daily averaged incident solar radiation at the surface, I_o is the solar constant, h_e is the depth of the euphotic layer (50 m), h is the depth of the mixed layer, P is the surface phosphate concentration (mol kg^{-1}), P_o is the half-saturation constant and T is the sea surface temperature (in °C). The temperature, light and mixed layer depth dependency terms followed the parameterization used by *Kurz and Maier-Reimer* [1993]. Our formulation of EP saturates at high phosphate concentrations, which is consistent with observations that high-phosphate regions do not respond to phosphate addition [*Sedwick et al.*, 1999]. In the OCM, the limiting nutrient is phosphate and adding phosphate to the upper ocean simulated macronutrient fertilization.

[22] In the model, the composition of the particulate organic matter (POM) assumed the classical Redfield ratio [*Redfield et al.*, 1963]

$$P : N : C : O_2 = 1 : 16 : 106 : 138. \quad (10)$$

The $CaCO_3$ export was a constant fraction of the organic matter export (8%). The exported POM from the euphotic layer was instantaneously remineralized below the euphotic layer. This implies that the sinking of POM greatly exceeds the effect of horizontal advection and no POM is advected out of the region where it is produced. For a course resolution model this is a valid assumption. To remineralize

POM, the vertical profile of POM is prescribed by the following equation

$$POM(z) = \left(\frac{z}{100m}\right)^{-a}, \quad (11)$$

where z is depth in meters and $a = 0.9$. This profile of POM is consistent with sediment trap data where observed values of a varied from 0.988 for particulate organic nitrogen to 0.858 for particulate organic carbon [*Martin et al.*, 1987]. In the model, POM that reaches the bottom is remineralized in the bottom layer. The remineralization of POM is allowed to occur under anoxic conditions, which is an important process in the eastern equatorial Pacific and the Gulf of Guinea. In anoxic conditions, POM is remineralized by denitrification. In the model, this occurs by allowing the remineralization of POM according to equation (11) without consuming oxygen.

[23] To remineralize $CaCO_3$, the vertical profile of $CaCO_3$ is given by the following equation

$$CaCO_3(z) = \exp^{-z/3500\,m}, \quad (12)$$

which is based on sediment trap data [*Martin et al.*, 1987]. With these prescribed profiles of POM and $CaCO_3$, POM is remineralized at shallower depths than $CaCO_3$.

[24] The BGC module allows for the exchange dissolved oxygen and CO_2 in the ocean with the atmosphere. Both the air-sea flux of O_2 and CO_2 were calculated using the wind speed and species-dependent gas exchange coefficient (K_{O2}, K_{CO2}) from *Wanninkhof* [1992] multiplied by the air-sea partial pressure difference between the surface ocean and the atmosphere.

$$\begin{aligned} Q_{o_2} &= K_{O2}\left(pO_2^{ocean} - pO_2^{atm}\right) \\ Q_{co_2} &= K_{CO2}\left(pCO_2^{ocean} - pCO_2^{atm}\right) \end{aligned}. \quad (13)$$

The partial pressure of O_2 in the atmosphere (pO_2^{atm}) was set to 20.85%. The partial pressure of O_2 in the ocean (pO_2^{ocean}) used the modeled surface ocean temperature and salinity, and the dissolved oxygen solubility equation of *Weiss* [1970]. The surface ocean pCO_2 was determined using the full carbon chemistry equations, which required modeled temperature, salinity, alkalinity, and dissolved inorganic carbon from the surface ocean. The steady state tracer distributions in the ocean were obtained by running the ocean model to steady state with initial average phosphate and alkalinity set to 2.1 μM and 2431 μM eq and the atmospheric CO_2 and O_2 set to 280 ppm and 20.85%.

3.3. Simulations

[25] The OCM was initially run to a quasi-steady state under preindustrial atmospheric CO_2 levels. From the preindustrial state (year 1850), model runs were made using a prescribed evolution of atmospheric CO_2 (Figure 3).

[26] The model predicts large regions in the upper ocean where macronutrients (phosphate) limit biological production (Figure 4), similar to those observed in the real ocean. The addition of macronutrients to these regions would stimulate marine biological export production and allow the ocean to sequester more atmospheric CO_2.

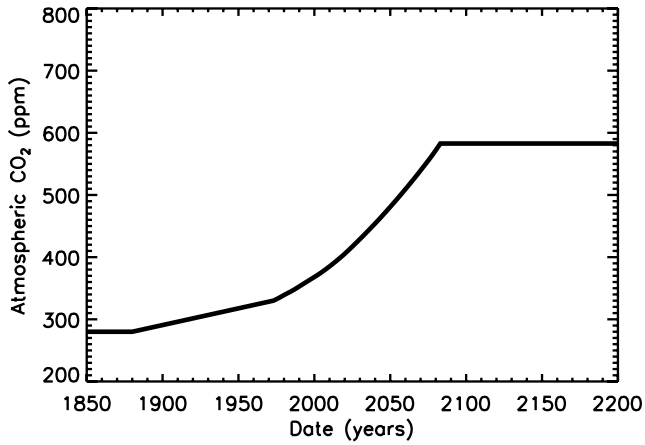

Figure 3. Prescribed evolution of atmospheric CO_2 used in the OCM runs.

[27] Phosphate fertilization runs were performed to investigate the potential of macronutrient fertilization to increase the ocean uptake of anthropogenic CO_2. For the fertilization runs, phosphate was added to the upper ocean of the 18°S to 50°S region at a constant rate of 1.2 Gt C equivalent/y. [For convenience all subsequent phosphate units are converted to carbon units by utilizing the carbon to phosphate ratio of the model (106) and quoted as equivalent carbon units]. Table 1, summarizes the model runs.

[28] Two different sets of experiments were performed with the model. The first set of experiments used the present seasonal climatology of sea surface temperature, salinity, wind speed, and sea ice extent as the forcing fields for the OCM. These experiments are referred to as results for the present climate. The second set of experiments used the same OCM, but the seasonal fields of sea surface temperature, salinity, wind speed, and sea ice extent were predicted using the CSIRO Climate Model under climate change simulation. This allowed us to investigate how modifications in the ocean circulation with climate change might alter the efficiency of macronutrient fertilization.

4. Ocean Carbon Model Results

4.1. Present Climate

[29] The box model represents the response of a phosphate-limited ocean to the addition of phosphate. The OCM should produce a similar response but with the following two complications. First, like the surface of the real ocean, the OCM has regions where biological production is not limited by macronutrients. In these regions, either the addition of phosphate or the transport of phosphate-enriched water into these regions will not increase export production. Second, in the OCM, the increased export production of organic matter is coupled to an increased export of calcium carbonate. This coupling between POM and $CaCO_3$ export reduces the oceanic CO_2 uptake because increased $CaCO_3$ export reduces alkalinity and the solubility of CO_2 of the surface water.

[30] In the OCM, phosphate fertilization stimulated the biological pump, increased the export of organic matter from the upper ocean and increased the ocean uptake of

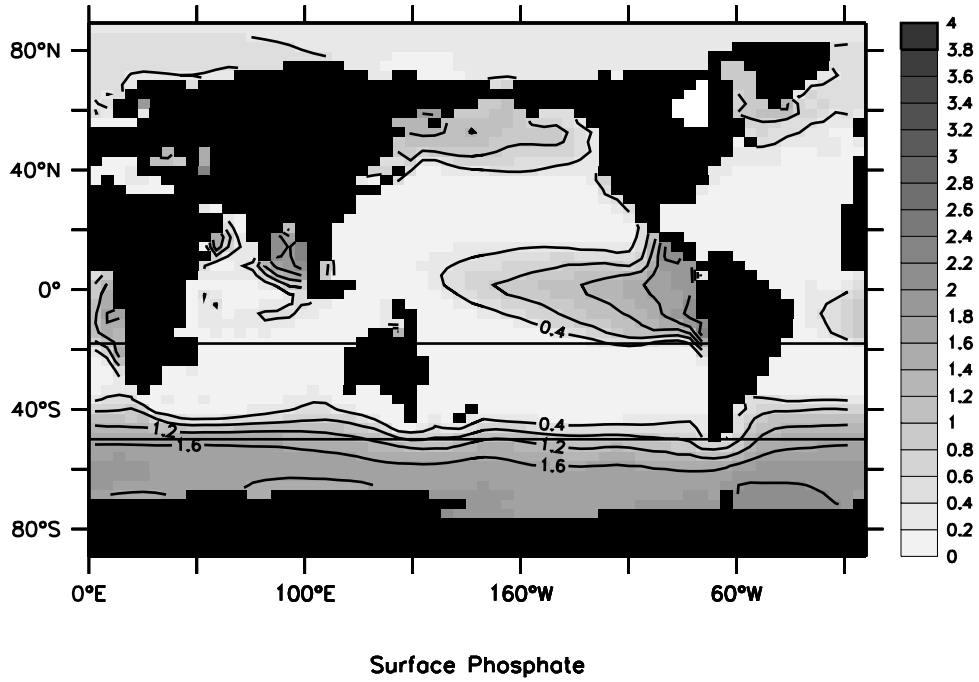

Figure 4. Annual averaged phosphate concentration in the surface ocean for the year 1999 of the control run. The box in the midlatitudes of the Southern Ocean denotes the fertilized region.

CO_2. Export production increased dramatically during the first 3 years of fertilization to 0.6 Gt C yr^{-1} (Figure 5). Following the period of rapid increase, export production continued to increase at nearly a constant rate for the remainder of the fertilization period and after 80 years of fertilization export production was 2.15 Gt C yr^{-1} greater than the prefertilization value. The temporal evolution of export production under phosphate fertilization in the OCM was consistent with the box model simulation. During the fertilization period, several decades are required before the export production equals the rate of phosphate addition (Figure 5b). Once the phosphate fertilization is stopped, export production declines but it takes several centuries for the export production to return to its prefertilized value.

[31] Phosphate fertilization increased the oceanic uptake of CO_2 (Figure 6). The increase in the ocean uptake of CO_2

Table 1. Model Runs Showing the Total Increase in Export Production, Oceanic Anthropogenic CO_2 Uptake and Atmospheric CO_2 Change[a]

Run	Fertilization Period	Enhanced Export Production, Gt C	Increased CO_2 Uptake, Gt C	Atmospheric CO_2 Change, μatm
Present Climatology: Response Between 2000 and 2200				
Control	none	–	–	
A	2000–2030	101	19	−9
B	2000–2050	162	31	−15
C	2000–2080	245	49	−24
D	2000–2080[1]	245	59	−28
E	none	–	–	
F	2000–2080			
G	2000–2080			
Present Climatology: Response Between 2000 and 2080				
Run C: Control	2000–2080	120.0	41.8	−21
Climate Change: Response Between 2000 and 2080				
Control climate	none	–	–	
Climate change	none	−65.3	−36.4	
Climate change with fertilization	2000–2080	63.3	7.4	
Impact of fertilization with climate change	2000–2080	128.6	43.8	−22

[a]Runs A, B, and C differ only in the length of the fertilization period. For runs D and E the calcium carbonate export was held at prefertilization levels. This was accomplished by not modifying the alkalinity equation. Run D differed from run E by being fertilized with phosphate between 2000 and 2080. Run F is equivalent to run C except that only regions with phosphate concentrations less than 0.4 μmol kg^{-1} are fertilized. Run G is identical to run F except that calcium carbonate production is held constant at the prefertilization level. The climate change runs were made using the CSIRO climate model and they showed the change between 2000 and 2080. The control climate run has no anthropogenic greenhouse forcing while the climate change runs use IS92a anthropogenic greenhouse gas concentrations (Figure 4).

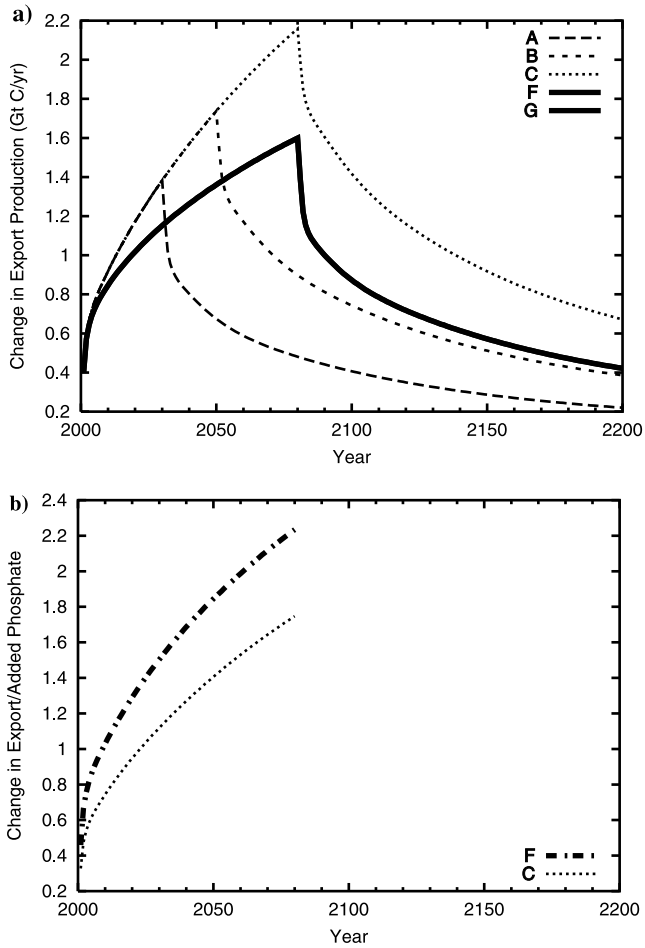

Figure 5. (a) Change in annual mean export production with time. (b) The ratio of annual mean export to annual phosphate addition (in carbon equivalent units).

rose dramatically at the start of phosphate fertilization but required 50 years before the oceanic CO_2 uptake stabilized to a new elevated value (Figure 6). The temporal response of the oceanic uptake of CO_2 in OCM to phosphate fertilization was consistent with the box model. The increase in the cumulative oceanic uptake of CO_2 during the 2000–2200 period from phosphate fertilization is summarized in Table 1.

[32] Once phosphate fertilization stopped, the oceanic uptake of CO_2 returned to the prefertilization value in less than 100 years. The return of the oceanic CO_2 uptake to the prefertilization value was much faster than the return of export production to its prefertilized value. The slower adjustment of the export production reflects the recycling of phosphate and carbon-enriched water in the upper ocean, which continues to affect export production without altering the oceanic CO_2 uptake.

[33] We defined the carbon sequestration efficiency of phosphate fertilization as the ratio of increased ocean uptake of CO_2 to the added phosphate in equivalent carbon units (equation (7)). For the OCM runs, the efficiency of phosphate fertilization never exceeded 48% (Figure 7, dashed line). The efficiency of the OCM was significantly less than the 86% efficiency predicted by the box model simulation (Figure 2). One may simply conclude that macronutrient

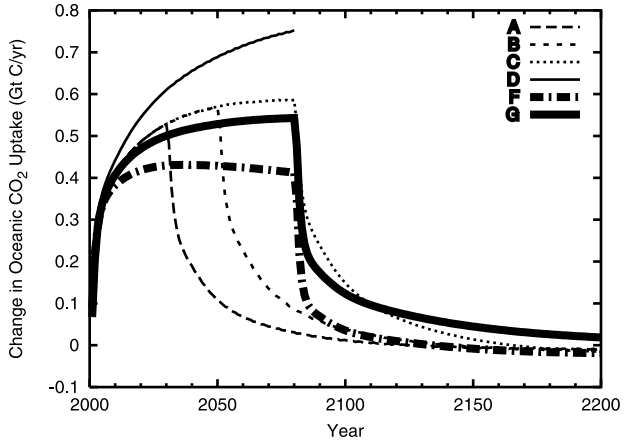

Figure 6. Change in the annual mean oceanic uptake of CO_2 from the control run for the various phosphate fertilization scenarios.

fertilization is not an efficient way to sequester anthropogenic CO_2 in the ocean. However, as stated at the start of this section, the OCM differed from the box model on two points: 1) phosphate addition stimulated both organic and calcium carbonate export from the upper ocean; 2) biological production is not limited by phosphate in all regions of the surface ocean.

[34] In the OCM, phosphate addition stimulated the export of both organic carbon and calcium carbonate from the upper ocean. Increased calcium carbon export reduces alkalinity, which reduces the solubility of dissolved CO_2 (gas) in seawater, and this reduces oceanic CO_2 uptake. In the OCM, the effect of increasing the calcium carbonate production was assessed using a model run where phosphate addition did not alter calcium carbonate production. With calcium carbonate production held constant, the maximum efficiency increased from 48% (run C) to 62% (run D) and the total CO_2 sequestered by the ocean increased from 49 Gt C to 59 GtC (20% increase). Calcium carbonate production has an important impact on the efficiency of CO_2 sequestration by phosphate fertilization.

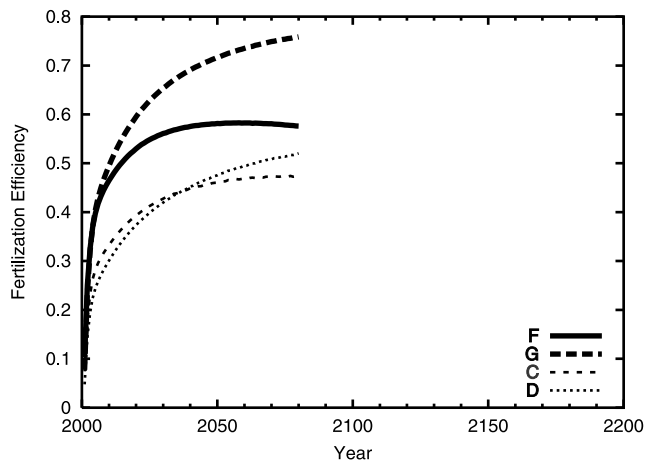

Figure 7. The ratio of the change in annual mean ocean CO_2 uptake to the annual mean phosphate addition in carbon equivalent units for the various runs.

[35] With calcium carbon production held constant, the maximum efficiency (62%) is still significantly less than the value predicted by the box model (86%). In the OCM, export production saturates at phosphate concentrations greater than 0.4 μmol kg^{-1}, hence adding phosphate to these regions produced no change in export production. Our export production formulation is consistent with observations from high-nutrient low-chlorophyll regions that demonstrate macronutrient addition to these regions does not stimulate biological production [*Boyd et al.*, 1996]. By indiscriminately adding phosphate to the entire 18°–50°S region, one fertilizes areas where export production was not phosphate-limited.

[36] To remove the effect of fertilizing water that is not phosphate-limited, we repeated the simulations, but only fertilized water in the 18°–50°S region that had surface phosphate concentrations less than 0.4 μmol kg^{-1}. With this fertilization scenario we simulated the impact of phosphate fertilization for the case where both export production and calcium carbon production increased (run F) and for the case where only export production increased (run G). As expected, limiting the region of phosphate fertilization increased the carbon sequestration efficiency. In run G, the carbon sequestration efficiency approached 78%, which is still less than the value predicted by the box model. The difference reflects the transport of the fertilized phosphate into regions that are not phosphate-limited. This feature is apparent when one compares the change in surface phosphate with the change in export production, and one sees phosphate increases in regions where there is no increase in export production (Figure 8). This loss of phosphate from the phosphate-limited ocean reduces the carbon sequestration efficiency of phosphate fertilization. It should be noted by restricting the phosphate fertilization to water with concentrations less than 0.4 μmol kg^{-1} the amount of phosphate added to the upper ocean is reduced and declines with time as the amount of phosphate in the upper ocean increases with time (Figure 9).

4.2. Climate Change

[37] Projections of climate change predict the ocean would experience sea surface warming, increased density stratification, reduced ventilation of the deep ocean and reduced supply of nutrient-rich water to the upper ocean [*Matear and Hirst*, 1999]. Such changes may alter the efficiency of phosphate fertilization. We performed simulations using the climate predictions from *Matear and Hirst* [1999] to assess whether phosphate fertilization response would change with climate change which are summarized in Table 1.

[38] Our fertilization simulation was made using a constant rate of phosphate addition of 1.2 Gt C yr^{-1} equivalent to the entire 18°–50°S region. With climate change, phosphate fertilization more than compensated for the reduction in both export production and oceanic CO_2 uptake predicted with climate change (Figure 10). By the year 2080 phosphate fertilization increased export production by 128.6 Gt C and oceanic CO_2 uptake by 43.1 Gt C. In comparison, by 2080 the present day climatology run predicted an export production increase of 120 Gt C and an oceanic CO_2 uptake of 41.8 Gt C. The small increased in ocean carbon sequestration and export production of the climate change run reflects the small increase (5%) in the area of the fertilized region that is phosphate-limited as compared to the present climate simulation.

5. Potential Impact of Macronutrient Fertilization

[39] As a consequence of stimulating biological productivity, macronutrient fertilization of the ocean would affect biogeochemical cycling of carbon, nutrients, and oxygen in the ocean with potential impacts on greenhouse gas concentrations in the atmosphere and the behavior of marine ecosystems. Changes in biogeochemical cycling caused by macronutrient fertilization and the possible marine ecosystem impacts are discussed in the following sections.

5.1. Carbon Chemistry

[40] The form of the macronutrients added to the seawater could alter the carbon chemistry. The addition of nitrogen as either dissolved nitric acid or dissolved ammonia would lower the seawater alkalinity and raise the fCO_2. The effect that nitric acid or ammonia addition has to the alkalinity of the ocean can used to estimate the how direct change in alkalinity cause by fertilization would impact the ability of the ocean to uptake CO_2. Using values from the surface water of the East Australia Current (total alkalinity of 2335 μM, fCO_2 of 313 μatm and a C/N of 106/16), the addition of nitric acid or ammonia would reduce the CO_2 uptake by 10% over the case where no alkalinity changes occur. In our macronutrient fertilization simulations, we assumed no change in alkalinity occurs with fertilization. This is equivalent to assuming that ammonium sulfate ($(NH_4)2SO_4$) is added to seawater to stimulate biological production. The addition of nitrogen in this form would not change the surface ocean alkalinity.

[41] As simulated in the OCM, macronutrient fertilization could increase calcium carbonate production, which would increase fCO_2 and offset the reduction in fCO_2 associated with increased export production. For a calcium carbonate to organic carbon ratio export ratio of 8% (value used in the OCM), the drop in fCO_2 due to increased export production would be reduced by approximately 10% because of the alkalinity decrease associated with increased calcium carbonate production. The $CaCO_3$:C_{org} ratio use for OCM simulations was low and an upper bound estimate for the global-averaged value is approximately 20% [*Shaffer*, 1993]. For a $CaCO_3$:C_{org} ratio of 20%, the drop in fCO_2 due to increased export production would be reduced by 25% because of increased calcium carbonate production.

[42] The response of the oceanic CO_2 uptake to changes in carbonate production can be amplified, because the dissolution of calcium carbonate is deeper than the remineralization of organic carbon. Hence the vertical resupply of alkalinity to the upper ocean under increased export is less than vertical resupply of dissolved inorganic carbon. In our OCM runs, changes in the calcium carbonate production reduced the maximum oceanic CO_2 uptake by 25%, which is more than double the reduction predicted from reduced alkalinity associated with increased calcium carbonate production (10%). The larger value in the OCM reflects the greater depth for the dissolution of calcium carbonate than for the remineralization of organic carbon,

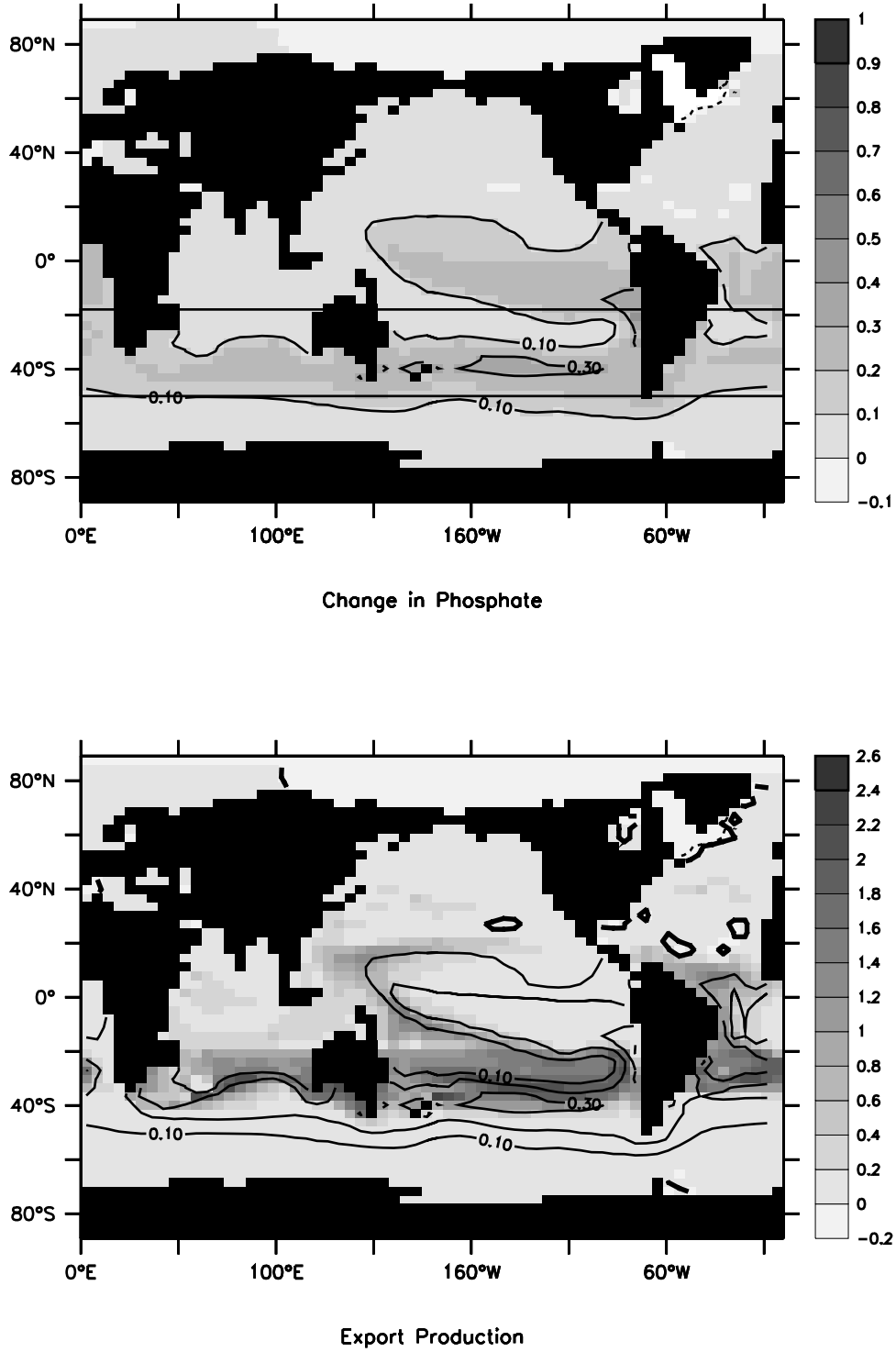

Figure 8. For run F at year 2080, after 80 years of phosphate fertilization the change in the annual mean export production. The contour lines denote the change in the annual mean surface phosphate concentration (μmol kg^{-1}). The box in the Southern Hemisphere denotes the region of phosphate fertilization.

which decouples the calcium carbonate cycle from the organic carbon cycle, and amplifies the impact of calcium carbonate production changes under phosphate fertilization. Increases in calcium carbonate production with phosphate fertilization may significantly reduce the CO_2 uptake efficiency. The OCM results highlight the need to assess the response of calcium carbonate producing organisms to macronutrient fertilization.

5.2. Oxygen Limitation and N_2O Production

[43] Macronutrient fertilization will increase the flux of organic matter into the ocean. Microbial respiration of this

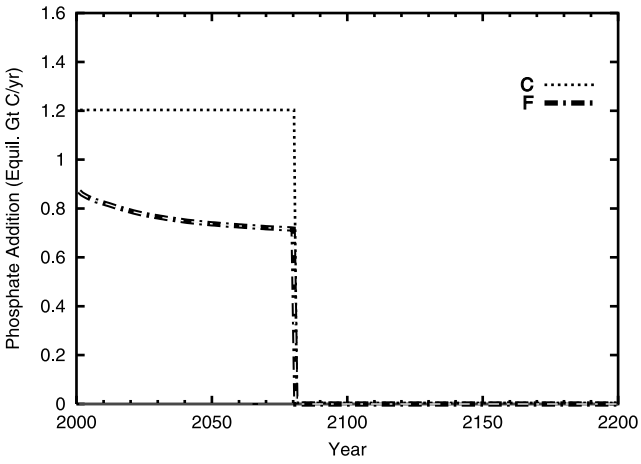

Figure 9. The rate of phosphate fertilization for runs A–D (dotted line) and for runs F and G (dash-dotted line) in equivalent carbon units.

organic material will deplete oxygen. Generally marine animals require oxygen to survive and anoxic regions (no dissolved oxygen) will be devoid of animal life. Mobile animals would avoid anoxic regions, but benthic organisms with limited mobility would die. In the control run, the highly productive equatorial upwelling regions contained layers of anoxic water (Figure 11). The presence of these anoxic layers is consistent with observations. With macronutrient fertilization, the thickness and extent of these layers increased. The change in the volume of anoxic water provided an indication of the impact of macronutrient fertilization (Figure 12). After 80 years of fertilization, the volume of anoxic water increased by 17.5%. The increase in anoxic water is generally confined to the equatorial Indian and Pacific oceans in the depth range of 1000–2000 m.

[44] Changes in the volume of low-oxygen or anoxic water will also alter microbial respiration of organic material producing N_2O and CH_4. Both N_2O and CH_4 are greenhouse gases with the ocean contributing 20% and 2% of the global emissions of these gases [*Houghton et al.*, 1995]. Any increased emissions of these greenhouse gases to the atmosphere due to macronutrient fertilization will offset the reduction in greenhouse warming of lower atmospheric CO_2. The weak ocean outgassing of CH_4 to the atmosphere from O_2-depleted regions indicates that CH_4 sources to the atmosphere are unlikely to increase under macronutrient fertilization and this prompts us to neglect this effect.

[45] We estimated the increased production of N_2O with macronutrient fertilization using two approaches. First, we related the increase in the N_2O production to the modeled increase in export production [e.g., *Fuhrman and Capone*, 1991]. With phosphate fertilization, export production increased by a maximum of 30%. Multiplying the current emissions of N_2O (3 Tg N yr^{-1}) by the increase in export production and converting this into the mass of N_2O (1.57) gives an increased emission of N_2O of 1.4 T g yr^{-1}. The change in N_2O emission can be converted to an equivalent amount of CO_2 emission by multiplying by 310 and by the carbon content of CO_2 (12/44) to yield 0.12 Gt C yr^{-1}. For the second calculation, the observation that N_2O is largely produced in low-oxygen water is used to assume that the change in the volume of low-oxygen water determined the increased production of N_2O. From the OCM runs, the volume of low-oxygen water increased by less than 20% and this equated to an increase in N_2O emissions of 1 T g yr^{-1}, equivalent to 0.08 Gt C yr^{-1} of CO_2 emissions.

[46] The emissions of N_2O would offset the increased oceanic CO_2 associated with phosphate fertilization runs by a maximum of 20%. Both our calculations of increased N_2O emissions are a simple attempt to estimate the negative feedback of macronutrient fertilization and more sophisticated model simulations would be need to explore this issue [e.g., *Subramaniam et al.*, 2002, 1999]. These two studies show that the N_2O production in the ocean is most consistent with the observed N_2O distribution when approximately half the production occurs in anoxic water and half is associated with the oxygen consumption due to organic matter remineralization. Our simple calculations of the N_2O feedback, which assumes all the N_2O production occurs either with oxygen consumption or in anoxic water, should

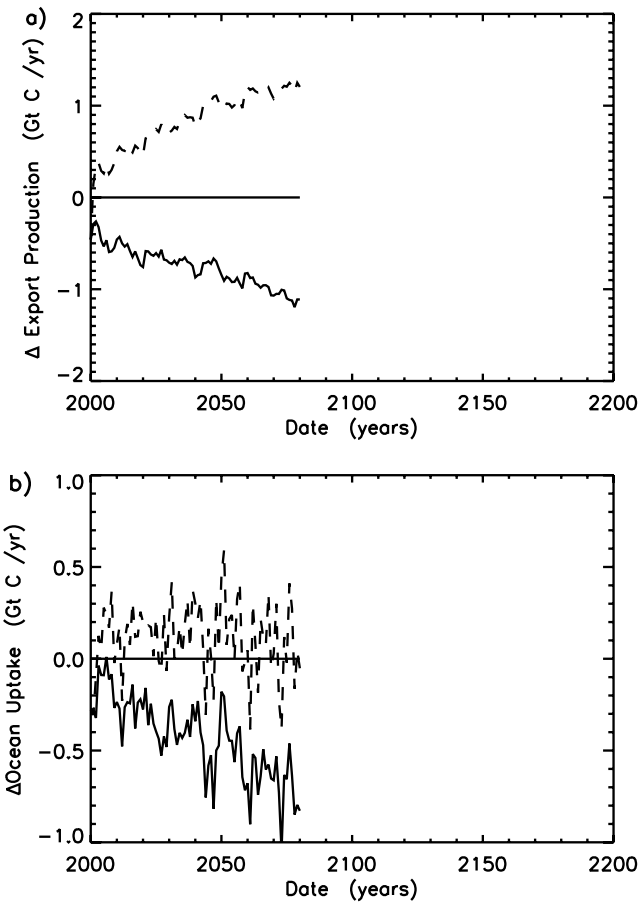

Figure 10. For the climate change simulations (a) the change in export production between the climate change run and the control run (solid) and between the climate change run with fertilization and the control run (dashed). (b) The change in oceanic CO_2 uptake between the climate change run and the control run (solid) and the climate change run with fertilization and the control run (dashed).

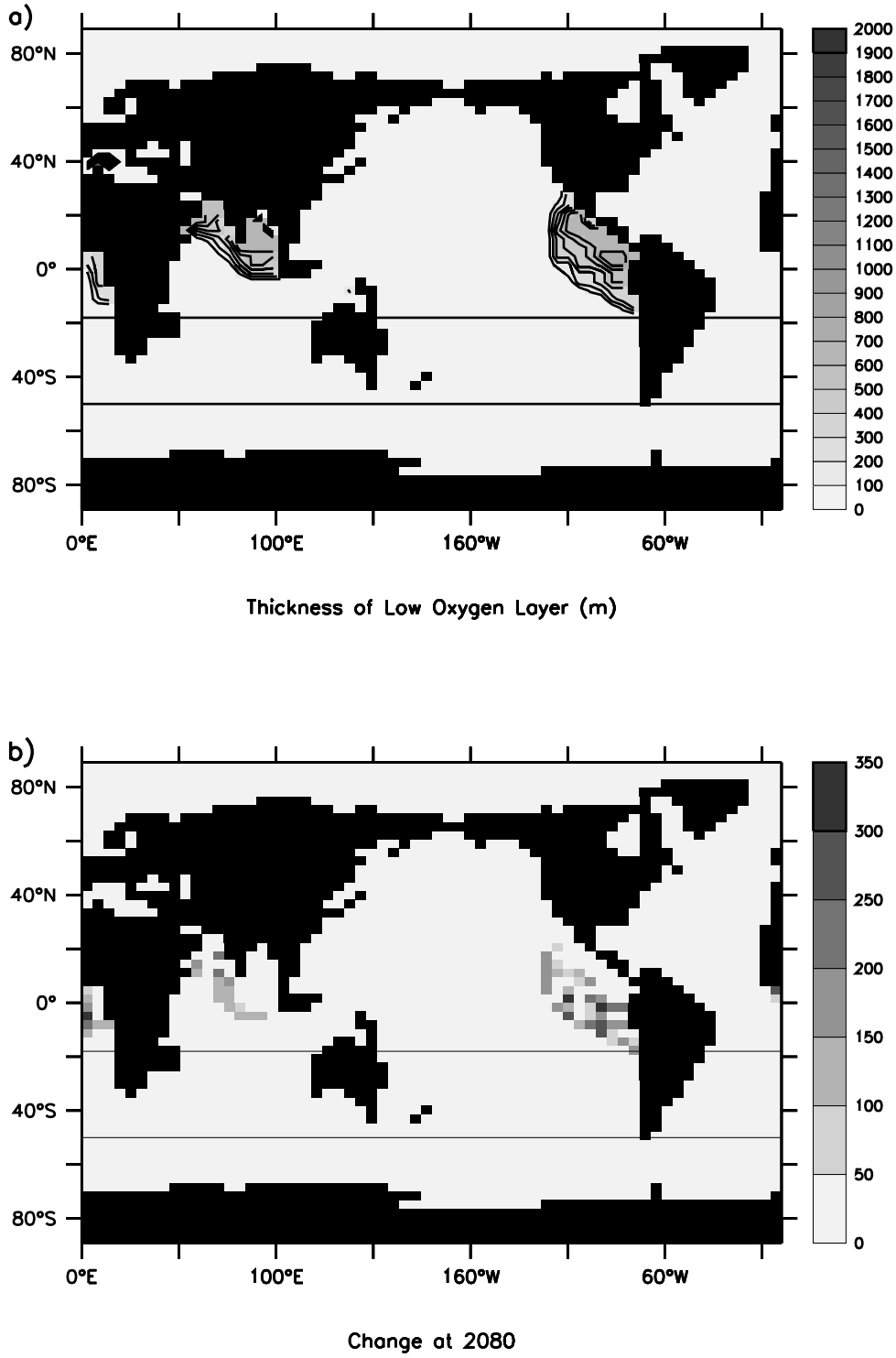

Figure 11. For the year 2080 (a) the thickness of the anoxic layer (m) in the control run and (b) the change in the thickness of the anoxic layer (m) between run C and the control run.

provide a reasonable estimate of the range in the N_2O affect on future greenhouse gas concentrations in the atmosphere.

[47] The potential for N_2O production to offset the greenhouse gas reduction associated with CO_2 uptake makes this a crucial process to further study. The fact that increased N_2O production may occur long after the fertilization stops further emphasizes the potential importance of this process at reducing the ability of macronutrient fertilization to reduce greenhouse gases in the atmosphere.

5.3. Phosphate Silicate and Iron Limitation

[48] In the subtropical gyres there is ample evidence to suggest that nitrate limits biological production and biological production would be stimulated by adding nitrate or

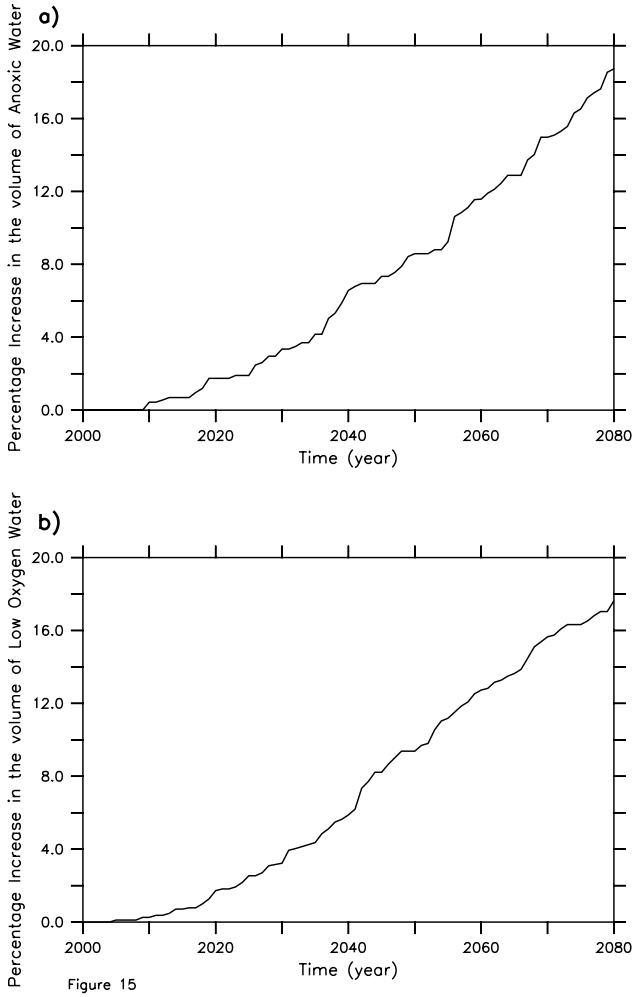

Figure 12. (a) The percentage increase in the volume of anoxic water (O_2 levels less than 1 μmol kg^{-1}) between run C and the control run and (b) percentage increase in the volume of low-oxygen water (O_2 levels between 1 and 10 μmol kg^{-1}) between run C and the control run.

ammonia to the surface ocean. Throughout the world oceans, the nitrate to phosphate ratio (N:P ratio) in deep water is nearly constant (N:P ratio equals 16:1) and approximately equal to the ratio of nutrient utilization by phytoplankton in the surface water [*Redfield et al.*, 1963]. At present, in the surface waters of the nitrate limited regions of the 18°–50°S oceans there is excess phosphate in the euphotic zone over the amount required to utilize all the nitrate of approximately 65×10^{10} moles P. For a C:N:P ratio of 106:16:1, the nitrogen required to deplete all the phosphate would be approximately 1040×10^{10} moles N and this would sequester approximately 0.8 Gt C. Any resupply of intermediate water to the upper ocean would contain a N:P ratio that was approximately Redfield, hence, it would not provide excess phosphate over nitrate. Therefore any nitrate only fertilization scheme would rapidly deplete all available phosphate. To justify fertilization of the ocean with macronutrients, one would want to sequester considerably more than 0.8 Gt C.

[49] If one drove the ecosystem from nitrate-limited to either phosphate-limited or silicate-limited, it would be expected that the species composition of the phytoplankton would change. The addition of both nitrate and phosphate would provide one option to avoid phosphate limitation, but the potential for silicate limitation would still exist and it needs to be assessed. The iron concentration in any fertilized region and its control on phytoplankton production would also needs to be known to ensure that one does not rapidly deplete the iron and switch the system from nitrate-limited to iron-limited.

5.4. DMS Production

[50] Most species of phytoplankton in the ocean produce dimethylsulphide (DMS), which is the dominant volatile sulphur-containing compound in the ocean and the major natural source of sulphur to the atmosphere [*Liss et al.*, 1997]. Marine DMS production can influence the radiative properties of the atmosphere by altering the albedo of clouds and by scattering incident solar radiation [*Charlson et al.*, 1987]. Changes in biological production in the ocean due to macronutrient fertilization could alter the DMS production in the ocean.

[51] The phytoplankton species composition and the activity of the microbial food web combined with primary productivity controls DMS production and its rate of release to the atmosphere [*Andreae*, 1990; *Kiene and Bates*, 1990]. Our knowledge of the large-scale response of ecosystem to macronutrient fertilization is inadequate at present to attempt to quantify changes in DMS production with ocean fertilization.

5.5. Marine Ecosystem Impacts

[52] The addition of macronutrients to oligotrophic regions would enhance biological production. The increased production may lead to increased fish catches but possible loss of species diversity. This may also alter the types of fish (i.e., shift from species typically caught in oligotrophic waters to species common in coastal or high-nutrient waters).

[53] Observations from the Baltic Sea and Hawaii Ocean Times-Series Sites provide guides to the possible marine ecosystem impacts of macronutrient fertilization. The Baltic Sea provides an example where large quantities of anthropogenic nitrate and phosphate have entered the sea. This has increased both primary production and pelagic fish catches. Associated with the increased biological production is the decline in oxygen levels in the deep water and the development of anoxic areas devoid of marine animals. Coastal regions of the Baltic Sea have experienced more frequent harmful blooms of algae (e.g., toxic bloom of *Chrysocromulina* [*Nielsen et al.*, 1990]). The consequences of anthropogenic macronutrients in the Baltic Sea are both positive and negative making it difficult to deduce the net benefit of anthropogenic nutrient enrichment.

[54] The Hawaii Ocean Time-Series (HOTS) provides insight into how marine ecosystems could respond to a shift from nitrate limitation to phosphate limitation. At HOTS, the marine ecosystem has undergone a shift from nitrate limitation to phosphate limitation in the last decade [*Karl et al.*, 1997]. This switch is the result of cyanobacteria (*Trichodesmium*) using N_2 fixation to satisfy their nitrate requirements. At present, the cyanobacteria supply half of the nitrogen required for new production. Cyanobacteria, like *Trichodesmium*, can grow with a reduced cell quota of

phosphorous which enables the ecosystem to drift to phosphorous limitation as the supply of new nitrogen switches from upwelling to the inexhaustible pool of N_2 dissolved in the surface ocean. Although *Trichodesmium* never dominate the phytoplankton population, they provide nitrogen essential for the non-nitrogen-fixing phytoplankton to grow more efficiently. With the switch from nitrate limitation to phosphate limitation, primary production at HOTS increased by 50% but particulate export production decreased by 30%. The switch to phosphate limitation increased the capacity of the ecosystem to recycle nutrients in the euphotic zone, which reduced the export of particulate organic matter and increased the accumulation of dissolved organic matter. For ocean fertilization, this suggests that driving the ecosystem to phosphate limitation may change the behavior of the ecosystem.

6. Conclusion

[55] The CO_2 sequestration efficiency of macronutrient fertilization of the ocean was investigated using a box model and a 3-D OCM. Both models employed phosphate as the only limiting macronutrient. The box model demonstrated that the maximum efficiency of phosphate fertilization would approach 86% for an oligotrophic region. In the OCM, the maximum efficiency of phosphate fertilization at stimulating CO_2 uptake approached 78%. The lower efficiency in the OCM reflects that in OCM some of the added phosphate is eventually transported to non-phosphate-limited regions and does not continue to stimulate export production and sequester carbon in the ocean.

[56] There are a number of processes that may efficiency of macronutrient fertilization in the ocean.

[57] 1. The form of the added macronutrients could reduce the efficiency of the sequestered carbon. By adding nitrogen in the form of either nitrate or ammonium one would reduce the alkalinity of the surface water and decrease the efficiency of carbon sequestration by 10%.

[58] 2. The potential for calcium carbonate export to alter the carbon sequestration efficiency of macronutrient fertilization. When calcium carbonate export was fixed at 8% of organic carbon export, the efficiency of carbon sequestered by macronutrient fertilization was reduced by 25% from the case where calcium carbonate production was held constant.

[59] 3. Increased oceanic outgassing of the greenhouse gas N_2O should occur with the increased biological production caused by fertilization. We estimate this could reduce the carbon sequestration efficiency by 20%.

[60] 4. The dramatic changes in ocean circulation predicted with climate change may alter carbon sequestration efficiency. Simulations with the OCM under an IS92a climate change scenario suggest that climate change does not alter the amount of carbon sequestered after 80 years of macronutrient fertilization.

[61] Considering these additional issues could reduce the maximum carbon sequestration efficiency to 43%, which is approximately half the value predicted by the idealized box model. Although, this minimum value is considered unlikely the large reduction from idealized box model results demonstrates that better understanding of the response of the marine system is needed to predict the carbon sequestration efficiency of macronutrient fertilization.

[62] The general discussion of the potential impact of macronutrient fertilization on biogeochemical cycling in the ocean and marine ecosystem identified a number of issues that need further study.

[63] One, the OCM predicted an increase of 17.5% in the volume of anoxic water after 80 years of fertilization. These increases in anoxic water were confined to regions that presently have large areas of anoxic water (e.g., eastern equatorial Pacific and Indian Ocean). Such a switch from oxic to anoxic conditions will alter the marine ecosystems in these regions.

[64] Two, a key question to address for any macronutrient fertilization scheme is whether both phosphate and nitrogen are required to enhance biological production in the ocean. Hypothesized macronutrient fertilization of the ocean has focused on adding only nitrogen to the ocean [*Jones*, 1999]. For regions of the Southern Hemisphere where nitrate limits production, the present available phosphate in the euphotic zone is approximately 65×10^{10} moles. Using the Redfield P:C ratio of 1:106, this suggests that only 0.8 Gt C can be sequestered before phosphate is exhausted. To sequester more that 0.8 Gt C requires the addition of both nitrogen and phosphate or phytoplankton must increase their N:P ratio. The latter response is highly speculative but ongoing work at the HOTS may provide further insight into the response of an oligotrophic ecosystem to the switch from nitrate limitation to phosphate limitation. The potential for the C:N:P requirement of phytoplankton to change greatly reduces our ability to model the ocean carbon cycle. This is a crucial issue to resolve [*Wong and Matear*, 1999], because it has important consequences on both the future ocean uptake of carbon and ocean fertilization schemes aimed at sequestering atmospheric carbon.

[65] Three, macronutrient fertilization will affect the radiative properties of the atmosphere by sequestering atmospheric CO_2 but there are a number of potential ocean feedbacks. Changes in carbonate production with macronutrient fertilization could directly influence the amount of atmospheric carbon that is sequestered. Our simulations demonstrate a large negative (25% reduction in sequestered carbon) influence of increased carbonate production on the amount of atmospheric carbon sequestered. Increased carbonate production may increase DMS production in the ocean, which may offset radiative effects of higher CO_2 in the atmosphere with higher DMS levels. Both these potential feedbacks are uncertain and require further investigation.

[66] Four, an additional change in the radiative properties of the atmosphere could be accomplished by altering the amount of N_2O transferred from the ocean into the atmosphere. *Fuhrman and Capone* [1991] hypothesized that increased biological production would increase the sea-air flux of N_2O. Using the modeled output, it was estimated that increased N_2O production could reduce the efficiency of macronutrient fertilization by a maximum of 20%. Our calculations are only approximations and further work is needed to reduce the uncertainties.

[67] Five, macronutrient fertilization has the potential to alter the structure of the phytoplankton community by increasing the biomass of phytoplankton or by shifting ecosystem production from a nitrogen-limited system to a phosphate-limited, a silicate-limited, or an iron-limited

system. The impact of these changes on higher trophic levels is uncertain. Ecosystems that are experiencing changes in the supply of macronutrients (i.e., HOTS and Baltic Sea) provide valuable sites to study the impact of macronutrient fertilization on marine ecosystems. Time series data from the Southern Hemisphere site would provide further insights into this impact.

[68] **Acknowledgments.** We are grateful to J. Davison and P. Freund for the valuable discussion of our research. The IEA Greenhouse Gas R&D Programme provided the funds for this project. Additional support to RJM was provided by the Australian Greenhouse Office.

References

Andreae, M. O. (1990), Ocean-atmosphere interactions in the global biogeochemical sulfur cycle, *Mar. Chem.*, *30*, 1–3.

Bacastow, R. B., and R. K. Dewey (1996), Effectiveness of CO_2 sequestration in the post-industrial ocean, *Energy Convers. Manage.*, *37*, 1079–1086.

Battle, M., M. L. Bender, P. P. Tans, J. W. C. White, J. T. Ellis, T. Conway, and R. J. Francey (2000), Global carbon sinks and their variability inferred from atmospheric O-2 and delta C-13, *Science*, *287*, 2467–2470.

Boyd, P. W., D. L. Muggli, D. E. Varela, R. H. Goldblatt, R. Chretien, K. J. Orians, and P. J. Harrison (1996), In vitro iron enrichment experiments in the NE subarctic Pacific, *Mar. Ecol. Prog. Ser.*, *136*, 179–193.

Bryan, K. (1984), Accelerating the convergence to equilibrium of ocean-climate models, *J. Phys. Oceanogr.*, *14*, 666–673.

Bryan, K., and L. J. Lewis (1979), A water mass model of the world ocean, *J. Geophys. Res.*, *84*, 347–376.

Charlson, R. J., J. E. Lovelock, M. O. Andreae, and S. G. Warren (1987), Oceanic phytoplankton, atmospheric sulphur, cloud albedo and climate, *Nature*, *326*, 655–661.

Coale, K. H., et al. (1996), A massive phytoplankton bloom induced by an ecosystem-scale iron fertilization experiment in the equatorial Pacific Ocean, *Nature*, *383*, 495–501.

Cox, M. D. (1987), Isopycnal diffusion in a z-coordinate ocean model, *Ocean Modell.*, *74*, 1–5.

England, M. H., and A. C. Hirst (1997), Chlorofluorocarbons uptake in a world ocean model: 2. Sensitivity to surface thermohaline forcing and subsurface mixing parameterizations, *J. Geophys. Res.*, *102*, 15,709–15,731.

England, M. H., J. S. Godfrey, A. C. Hirst, and M. Tomczak (1993), The mechanism for antarctic intermediate water renewal in a world ocean model, *J. Phys. Oceanogr.*, *23*, 1553–1560.

Fuhrman, J. A., and D. G. Capone (1991), Possible biogeochemical consequences of ocean fertilisation, *Limnol. Oceanogr.*, *36*, 1951–1959.

Gent, P. R., and J. C. McWilliams (1990), Isopycnal mixing in ocean circulation models, *J. Phys. Oceanogr.*, *20*, 150–155.

Gent, P. R., J. Willebrand, T. J. McDougall, and J. C. McWilliams (1995), Parameterizing eddy-induced tracer transports in ocean circulation models, *J. Phys. Oceanogr.*, *25*, 463–474.

Hellerman, S., and M. Rosenstein (1983), Normal monthly wind stress over the world ocean with error estimates, *J. Phys. Oceanogr.*, *13*, 1093–1104.

Hirst, A. C., and T. J. McDougall (1996), Deep-water properties and surface buoyancy flux as simulated by a z-coordinate model including eddy-induced advection, *J. Phys. Oceanogr.*, *26*, 1320–1343.

Houghton, J. T., , L. G. M. Filho, J. Bruce, H. Lee, B. A. Callander, E. Haites, N. Harris, and K. Maskell (Eds.) (1995), *Climate Change, 1994*: *Radiative Forcing of Climate Change and an Evaluation of the IPCC IS92 Emission Scenarios*, 334 pp., Cambridge Univ. Press, New York.

Jones, I. S. F. (1999), Lowering the cost of carbon sequestration by ocean nourishment, in *Greenhouse Gas Control Technologies*, edited by B. Eliasson, P. Riemer, and A. Wokaun, pp. 255–259, Pergamon, New York.

Joos, F., J. L. Sarmiento, and U. Siegenthaler (1991), Estimates of the effect of Southern Ocean iron fertilization on atmospheric CO_2 concentrations, *Nature*, *349*, 772–775.

Karl, D., R. T. L. Leteiler, J. Dore, J. Christian, and D. Hebel (1997), The role of nitrogen fixation in biogeochemical cycling in the subtropical North Pacific Ocean, *Nature*, *388*, 533–538.

Keeling, R. F., S. C. Piper, and M. Heimann (1996), Global and hemispheric CO_2 sinks deduced from changes in atmospheric O_2 concentrations, *Nature*, *381*, 218–221.

Kiene, R. P., and T. S. Bates (1990), Biological removal of dimethyl sulphide from sea water, *Nature*, *345*, 702–705.

Kurz, K. D., and E. Maier-Reimer (1993), Iron fertilization of the austral ocean—The Hamburg model assessment, *Global Biogeochem. Cycles*, *7*, 229–244.

Levitus, S. (1982), Climatological atlas of the world ocean, *NOAA Prof. Pap 13*, U. S. Govt. Print. Off., Washington, D. C.

Liss, P. S., A. D. Hatton, G. Malin, P. D. Nightingale, and S. M. Turner (1997), Marine sulphur emissions, *Philos. Trans. R. Soc. London, Ser. B*, *352*, 159–168.

Martin, J. H., G. A. Knauer, D. M. Karl, and W. W. Broenkow (1987), VERTEX: The carbon cycling in the northeast Pacific, *Deep Sea Res., Part A*, *34*, 267–285.

Matear, R. J. (2001), Effects of eddy parameterizations and numerical advection schemes on ocean ventilation and anthropogenic CO_2 uptake of a ocean general circulation model, *Ocean Modell.*, *3*, 217–248.

Matear, R. J., and A. C. Hirst (1999), Climate change feedback on the future oceanic CO_2 uptake, *Tellus, Ser. B*, *51*, 722–733.

Matear, R. J., and C. S. Wong (1999), Potential to increase the oceanic CO_2 uptake by enhancing marine productivity in high nutrient low chlorophyll regions, in *Greenhouse Gas Control Technologies*, edited by B. Eliasson, P. Riemer, and A. Wokaun pp. 249–253, Pergamon, New York.

Nielsen, T. G., T. Kiorboe, and P. Bjornsen (1990), Effects of a Chrysochromulina polylepis sursurface bloom on the planktonic community, *Marine Ecology - Progress Series*, *62*, 21–35.

Orr, J., and J. L. Sarmiento (1992), Potential of marine macroalgae as a sink for CO_2: Constraints from a 3-D general circulation model of the global ocean, *Water Air Soil Pollut.*, *64*, 405–421.

Peng, T.-H., and W. Broecker (1991), Dynamical limitations on the Antarctic iron fertilization strategy, *Nature*, *349*, 227–229.

Redfield, A., B. Ketchum, and F. Richards (1963), The influence of organisms on the composition of sea water, in *The Sea*, edited by M. Hill, pp. 26–77, Interscience, New York.

Rix, N. H., and J. Willebrand (1996), Parameterization of mesoscale eddies as inferred from a high-resolution circulation model, *J. Phys. Oceanogr.*, *26*, 2281–2285.

Sarmiento, J. L., and J. C. Orr (1991), Three-dimensional simulation of the impact of the Southern Ocean nutrient depletion on atmospheric CO_2 and ocean chemistry, *Limnol. Oceanogr.*, *36*, 1928–1950.

Sedwick, P. N., G. R. DiTulliio, D. A. Hutchins, P. W. Boyd, F. B. Griffiths, A. C. Crossley, T. W. Trull, and B. Quéguiner (1999), Limitation of algal production by iron and silicic acid deficiency in the Australian Subantarctic region, *Geophys. Res. Lett.*, *26*, 2865–2868.

Shaffer, G. (1993), Effects of the marine biota on global carbon cycling, in *The Global Carbon Cycle*, edited by M. Heimann, pp. 431–455, Springer-Verlag, New York.

Subramaniam, A., E. J. Carpenter, and P. G. Falkowski (1999), Bio-optical properties of the marine diazotrophic cyanobacteria *Trichodesmium* spp. II. A reflectance model for remote sensing, *Limnol. Oceanogr.*, *44*, 618–627.

Subramaniam, A., C. W. Brown, R. R. Hood, E. J. Carpenter, and D. G. Capone (2002), Detecting Trichodesmium blooms in SeaWiFS imagery, *Deep Sea Res., Part II*, *49*, 107–121.

Wanninkhof, R. (1992), Relationship between wind speed and gas exchange over the ocean, *J. Geophys. Res.*, *97*, 7373–7382.

Weiss, R. F. (1970), The solubility of nitrogen, oxygen and argon in water and seawater, *Deep Sea Res.*, *17*, 721–735.

Wong, C. S., and R. J. Matear (1995), Carbon sequestration by the Marine Biota, in *Carbon Sequestration in the Biosphere*, edited by M. Beran, pp. 19–31, Springer-Verlag, New York.

Wong, C. S., and R. J. Matear (1997), Ocean disposal of CO_2 in the North Pacific Ocean: Assessment of CO_2 chemistry and circulation on storage and return to the atmosphere, *Waste Management*, *17*, 329–336.

Wong, C. S., and R. J. Matear (1999), Sporadic silicate limitation of phytoplankton productivity in the subarctic northeast Pacific, *Deep Sea Res., Part II*, *46*, 2539–2556.

B. Elliott and R. J. Matear, CSIRO Marine Research, GPO Box 1538, Hobart, Tasmania, Australia, 7001. (richard.matear@csiro.au)